Applied Surface Science xxx (2009) xxx–xxx

Contents lists available at ScienceDirect

Applied Surface Science

journal homepage: www.elsevier.com/locate/apsusc

Femtosecond laser ablation of silver foil with single and double pulses

D.E. Roberts [a,*], A. du Plessis [a,b], L.R. Botha [a,b]

[a] CSIR National Laser Centre, PO Box 395, Meiring Naude Road, Pretoria 0001, South Africa
[b] Physics Department, University of Stellenbosch, Private Bag X1, Matieland 7602, South Africa

ARTICLE INFO

Article history:
Received 11 August 2009
Received in revised form 1 October 2009
Accepted 3 October 2009
Available online xxx

Keywords:
Femtosecond metal ablation
Double pulse ablation
Nanoparticle deposition
Femto-LIBS
Silver nanoparticles

ABSTRACT

The average ablation depth per pulse of silver foil by 130 fs laser pulses has been measured in vacuum over a range of three orders of magnitude of pulse fluence up to 900 J cm^{-2}. In addition, double pulses with separations up to 3.4 ns have been used to probe time scales of relevance for femtosecond ablation. The double pulse ablation depth, when each pulse fluence is 0.7 J cm^{-2}, falls to that of a single pulse as the pulse separation is increased from 0 ps to 700 ps. This time scale decreases to only 4 ps as the fluence is increased to 11 J cm^{-2}. It then jumps to 500 ps across a transition fluence where the slope of the ablation depth versus logarithmic fluence characteristic changes abruptly to a higher value. In addition, for pulse separations near 1000 ps, the second pulse can cause re-deposition of ejecta from the first pulse resulting in a double pulse ablation depth only 40% that of the first pulse alone. This has important implications for the interpretation of double pulse femto-LIBS intensities. Our results suggest that the optical properties of nano or mesoparticles play a significant role in double pulse ablation with large pulse separations.

1. Introduction

A fundamental problem in femtosecond laser ablation is to understand how the removed depth per pulse, d, depends on the laser fluence, F, as well as other laser and material parameters. A two temperature model, with the assumption that vapourisation was the removal mechanism, was successful in predicting experimentally observed results for metals [1,2]:

$$d = K \ln\left(\frac{F}{F_{th}}\right) \quad (1)$$

where F_{th} is the threshold fluence for ablation and K is a constant.

Moreover, the model predicted, as observed, two ablation regimes. One had a low F_{th} (≈0.14 J cm^{-2} for copper) and small K (≈10 nm) of about the optical penetration depth of the laser radiation in the metal. The second regime had a higher F_{th} (≈0.46 J cm^{-2} for copper) and larger K (≈80 nm) of about an electron heat conduction length [2]. Several experimental studies on different metals confirmed the logarithmic dependence on fluence of the ablation depth as well as the existence of two different regimes [3–7].

In spite of the success of the basic two temperature with vapourisation model, many details of femtosecond metal ablation remain unclear. In particular, all the transport parameters in the model are in a highly non-equilibrium regime and are not known in general [3,8,9]. Also, the mechanisms of removal are not well established [10–14]. These could include vapourisation, phase explosion, spallation, fragmentation, etc., or a combination of mechanisms. In addition, the absorption and penetration of the laser light is not expected to follow simple classical laws [15,16]. These problems continue to stimulate further studies of femtosecond ablation.

For example, more recent experimental results have shown other fluence regimes than the two noted above: an even lower fluence regime with $F_{th} \approx 0.018$ J cm^{-2} for copper [5], though not a good fit to Eq. (1), and a higher fluence regime above about 30 J cm^{-2}, also for copper [17].

In the present work, we have measured the *average* ablation depth in 25 μm and 50 μm thick silver foils over a very wide range of incident fluences, from 0.3 J cm^{-2} to 900 J cm^{-2}, in particular concentrating on the transition regions between different ablation regimes. We have also used a range of lens focal lengths to see whether spot size on the sample as well as peak fluence is an important parameter. In addition, we have used double pulses with separations of up to 3.4 ns in a pump probe experiment to study a transition region between two logarithmic fluence regimes.

Fairly extensive experimental results have been reported on "single pulse" femtosecond metal ablation, though few specifically on silver [3,7] but results on dual (or multiple) pulse ablation have been rather more limited [18–31]. By dual pulse it is always understood that the pulse separation is much less than the inter-pulse period (typically 1 ms) of the train of amplified femtosecond

* Corresponding author. Tel.: +27 12 841 4851; fax: +27 12 841 3152.
E-mail address: troberts@csir.co.za (D.E. Roberts).

0169-4332/$ – see front matter © 2009 Elsevier B.V. All rights reserved.
doi:10.1016/j.apsusc.2009.10.004

pulses used for ablation. While there has been much overlap in the aims of various studies, these can be broadly divided into several groups.

For large pulse separations (>ns) multiple pulses can be used to increase the ablation depth compared with a single pulse of the same total energy [6]. This is because the single pulse ablation depth increases more slowly than linearly with fluence (Eq. (1)). One objective of having dual or multiple pulses with small separations (<10 ps) can be to reduce the peak laser intensity in order to avoid air breakdown for a given total pulse energy [6]. Double pulses have also been used to try and improve the quality of laser materials processing [18–20].

In femtosecond laser-induced breakdown spectroscopy (LIBS), the optimum pulse separation is usually ~several 100 ps. Here the objective of the second pulse is not specifically to increase the ablation depth but rather to reheat the plasma created by the first pulse. This increases the emission intensity of the plasma and thereby improves the signal to noise ratio compared with a single pulse LIBS measurement [21–25].

Finally, as in the present study, a second pulse can be used to probe conditions generated by the first pulse on a wide range of time scales. These can range from electron lattice relaxation times or electron diffusion times (a few ps to a few 100 ps) to times for the development of the ablation plume (up to a few 1000 ps) [26–31].

2. Theoretical background

We used the basic one-dimensional, two temperature, femtosecond ablation model [1] to calculate the time dependence of the electron temperature, T_e, and the lattice temperature, T_i, as a function of distance, z, into the material. Specifically, we are interested in the double pulse ablation depth as a function of pulse separation and fluence, as well as the behaviour of the ablation depth across a change in fluence regimes to compare with experimental results described later.

If both pulses have the same incident flat-top intensity, I, of duration τ_L and the second one is delayed by τ_S with respect to the first, the model is

$$C_e\frac{\partial T_e}{\partial t}=\frac{\partial}{\partial z}\left(K_e\frac{\partial T_e}{\partial z}\right)-g(T_e-T_i)+I(t)(1-R)\alpha e^{-\alpha z}+P_T I(t-\tau_S)(1-R)\alpha e^{-\alpha z} \quad (2)$$

$$C_i\frac{\partial T_i}{\partial t}=g(T_e-T_i) \quad (3)$$

where $I(t)=0$ for $t>\tau_L$ and $I(t-\tau_S)=0$ for $t>\tau_S+\tau_L$. C_e and C_i are the electron and lattice heat capacities, K_e is the electron thermal conductivity, g is the electron–lattice coupling parameter, R is the reflection coefficient and α is the absorption coefficient of the material. P_T is the fraction of the intensity of the second pulse transmitted to the material through the ejected matter and/or plasma of the first pulse. Calculations were made with C_e and g from Ref. [32] and other parameters from Ref. [3].

We find that for a single pulse ($P_T=0$) the heat diffusion term is not negligible even during the short duration of the pulse (for $t_L=130$ fs) so that the penetration scale length of the electron temperature is significantly greater than the skin depth, α^{-1}, at $t=\tau_L$. Nevertheless, for simplicity we assume there is no diffusion up to τ_L so the initial boundary conditions at $t=\tau_L$ are

$$T_e=\sqrt{\frac{2(1-R)F\alpha}{C_e'}}\exp\left(\frac{-\alpha z}{2}\right)\quad\text{and } T_i=300\,\text{K} \quad (4)$$

Here $F=I\tau_L$ is the *incident* pulse fluence and $C_e'=C_e/T_e$ is assumed to be constant. We then solve the above equations for the *surface temperatures only*, $T(0,t)$, matching the exact calculation for small times with the long term solution for a δ function surface heat deposition [33]:

$$T_e(z,t)=\frac{2(1-R)\delta F}{C_e\sqrt{4\pi D_e t}}\exp\left(\frac{-z^2}{4D_e t}\right) \quad (5)$$

We take the threshold fluence for ablation as when the surface temperature exceeds a fixed value, T_{ab} [2]. We assume phase explosion is the ablation mechanism so the appropriate T_{ab} would be near the critical temperature, T_{cr}, from the liquid–vapour interface criterion. The value of T_{cr} is not clear [13,10,34] so we take $T_{ab}=5000$ K for silver. The conclusions drawn later are not at all dependant on this choice. In order to match the threshold fluence from the model with the measured threshold incident fluence of 0.56 J cm^{-2} it was necessary to use $R=0.97$, considerably different from the Fresnel value of $R=0.99445$ at 795 nm, i.e. $(1-R)$ was five times higher than the classical value for pure silver. This adjustment of the Fresnel value has previously found to be necessary in calculations [33] and in matching multiple pulse with single pulse measured ablation thresholds [35]. The increase in absorptivity is probably due to roughened and damaged surfaces from previous pulses, but could also be influenced by the strong changes in electron temperature during the pulse, not included in the present analysis.

Double pulse calculations with the above model for an incident fluence of 0.65 J cm^{-2} per pulse and four different pulse separations are shown in Fig. 1. The main timescales of interest for a single pulse can be seen in Fig. 1(a) (i.e. $\tau_S=0$) and as a function of fluence in Fig. 2. Fig. 2(a) shows τ_{ei}, the time for T_i to reach 99% of T_e, in the absence of electron diffusion ($K_e=0$). Except near threshold, it is only weakly dependent on fluence for the transport parameters used here and is approximately equal to 20 ps. The strong electron diffusion reduces τ_{ei} by a factor of two to about 10 ps (Figs. 2(b) and 1(a)). Fig. 2(c) shows the time for the surface lattice temperature to reach the ablation temperature, T_{ab}. Fig. 2(d) gives the time at which T_i falls below T_{ab}. The latter is included for completeness though without a treatment of the ablation mechanism the model is particularly unrealistic for large times. The two extreme curves (c) and (d) meet at τ_{ei} for the threshold fluence. In this model, the peak temperature is reached at a time $\approx\tau_{ei}$.

The effect of increasing pulse separation on the maximum surface temperature is shown in Figs. 1 and 3. For $\tau_S\leq\tau_{ei}$ (Figs. 1(a)–(c) and 2) there is relatively little change in the peak temperature with τ_S. At longer times there are separate peaks from the two pulses and the maximum temperature from the second pulse falls monotonically to the single pulse peak temperature on a timescale determined by lattice diffusion (Figs. 1(d) and 3). This is because, for $t>\tau_{ei}$, the surface temperature due to the first pulse is falling when the second pulse reaches the surface.

Of course this model takes no account of what happens due to phase changes in the material between the first and second pulses. For $\tau_S\gg$ a few 100 ps (cf. Fig. 1(d)) the pulses are completely separate and each will cause the maximum temperature rise of a single pulse, again in so far as conditions created by the first pulse, such as plasma formation, do not interfere with the transmission of the second pulse to the surface.

From Figs. 1–3 we can therefore identify different regimes for τ_S:

1. For $\tau_S\ll\tau_{ei}$, the two pulses, each of fluence F behave as a single pulse of fluence $2F$ (with an ablation depth per pulse as (1), $d=K\ln(2F/F_{th})$.
2. For $\tau_S\leq\tau_{ei}$, the surface temperature and therefore the predicted ablation depth is almost independent of τ_S, the exact value

Please cite this article in press as: D.E. Roberts, et al., Femtosecond laser ablation of silver foil with single and double pulses, Appl. Surf. Sci. (2009), doi:10.1016/j.apsusc.2009.10.004

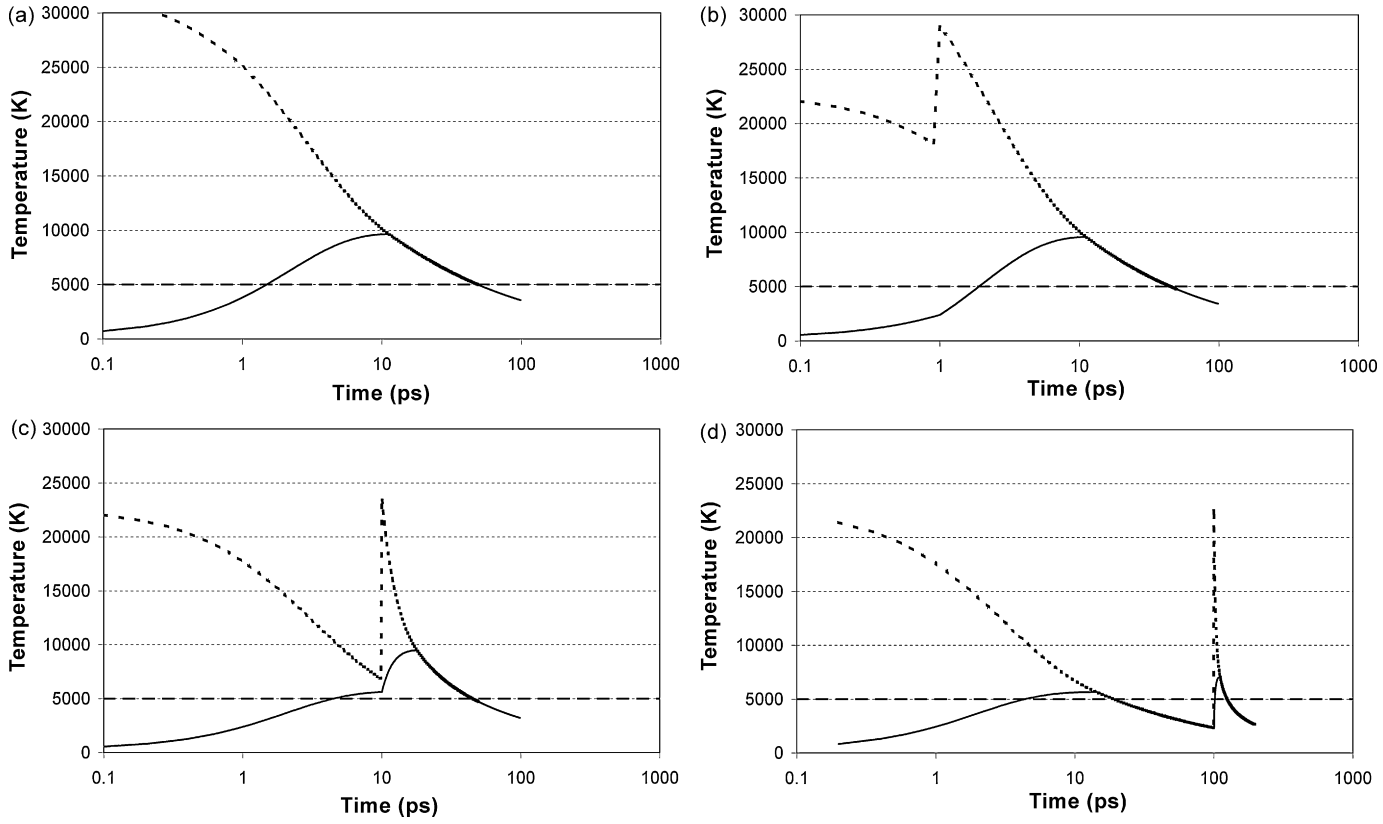

Fig. 1. Surface temperature versus time calculated for double pulse ablation with a fluence of 0.65 J cm^{-2} per pulse and pulse separations (a) 0 ps, (b) 1 ps, (c) 10 ps and (d) 100 ps. Short dashes: electron temperature; solid curve: surface lattice temperature; long dashes: ablation temperature.

depending on the specific values and temperature dependences of γ, K_e and C_e.

3. For $\tau_{ei} < \tau_S < \tau_D$, where τ_D is a characteristic time for heat diffusion, the surface temperature and the predicted ablation depth fall with increasing τ_S.
4. For $\tau_S \sim \tau_T$ where τ_T is a characteristic time for ejecta from the first pulse to interfere with the second pulse (i.e. reduce P_T to below 1), the ablation depth can be expected to be less than for regimes 1–3. If τ_T corresponds to plasma formation (where typically $\tau_T > \tau_D$) the second pulse could simply reheat the plasma formed by the first pulse but not increase the ablation depth at all ($P_T = 1$) so $d = K \ln(F/F_{th})$. This is the regime of interest in LIBS. However, as seen in the experimental results, we can have $\tau_T \sim \tau_D$ and $P_T < 1$ so that the regime with $P_T < 1$ can overlap with regime 3.
5. For $\tau_S \gg \tau_{ei}$, τ_D, τ_T, the pulses are essentially independent so the ablation depth is simply the sum of the individual pulse depths, $d = 2K \ln(F/F_{th})$.

We are also interested in the ablation depth as a function of fluence across a transition from a regime A where $d = K \ln(F/F_A)$ to a regime B where $d = K \ln(F/F_B)$ at a fluence F_{AB} defined by $K_A \ln(F_{AB}/F_A) = K_B \ln(F_{AB}/F_B)$. This corresponds to the measurements described below where d varies continuously through F_{AB} but there is a change in slope of the d versus $\ln(F)$ characteristic from K_A to K_B.

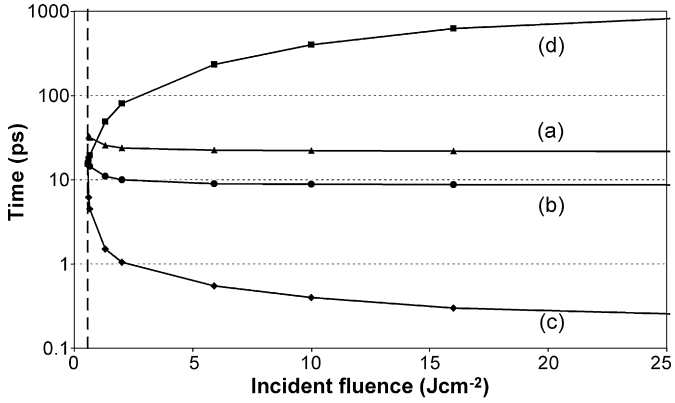

Fig. 2. Lattice surface temperature times scales as a function of incident fluence for single pulse ablation (the dashed line is at threshold). (a) Time for lattice temperature to reach 99% of electron temperature with no electron diffusion. (b) As (a) but with electron diffusion. (c) Time to reach ablation temperature, T_{ab}. (d) Time for lattice temperature to fall below T_{ab}.

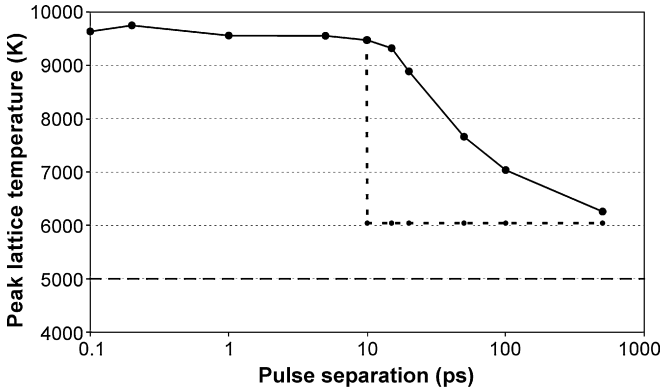

Fig. 3. Solid line: maximum surface lattice temperature as a function of pulse separation for a fluence of 0.65 J cm^{-2} per pulse. After 10 ps there are peaks from the first and second pulses. The short dashes show the peak temperature from first pulse. Long dashes: ablation temperature.

Please cite this article in press as: D.E. Roberts, et al., Femtosecond laser ablation of silver foil with single and double pulses, Appl. Surf. Sci. (2009), doi:10.1016/j.apsusc.2009.10.004

For pulse separation regime (1) above, the ratio of double to single pulse ablation across a transition has the form:

$$\begin{aligned} d(2F)/d(F) &= 1 + \ln(2)/\ln(F/F_A) && \text{for } F \le F_{AB}/2 \\ &= K_B/K_A \ln(2F_B)/\ln(F_A) && \text{for } F_{AB}/2 \le F \le F_{AB} \\ &= 1 + \ln(2)/\ln(F/F_B) && \text{for } F \le F_{AB} \end{aligned} \quad (6)$$

This ratio is shown as a function of fluence in Fig. 4(a) for $K_A = 109$ nm, $F_A = 0.57$ J cm^{-2}, $K_B = 471$ nm and $F_B = 4.4$ J cm^{-2} corresponding to measurements described below. For a fluence near the single pulse threshold, $F \to F_A$, $d(2F)/d(F) \to \infty$. However, $d(2F)$ is still finite if $2F > F_A$.

In pulse separation regimes (2) and (3), the ratio will depend on τ_{ei} and τ_D, while in regime (4) for $P_T = 1$, $d(2F) = K \ln(F/F_{th})$ and $d(2F)/d(F) = 1$ (Fig. 4(b)). In regime (5) $d(2F) = 2K \ln(F/F_{th})$ and $d(2F)/d(F) = 2$ (Fig. 4(c)). This differs from regime (1) as $2K \ln(F/F_{th}) \neq K \ln(2F/F_{th})$ in general.

3. Experimental details

The laser was a standard Ti:Sapphire system comprising an oscillator (Coherent, model Mira 900F) and an amplifier (Coherent, model Legend). The amplified pulses were of 130 fs duration at a central wavelength of 795 nm and energies up to 1.05 mJ at a repetition rate of 1 kHz. The pre- and post-pulses were adjusted to be <0.2% and <1% respectively of the main pulse. Also, measurements with a fast photodiode (risetime 0.35 ns) that could distinguish between the (un-resolved) femtosecond pulse and an amplified spontaneous emission background (duration a few ns) indicated no significant energy in the latter.

The beam was focussed on a 99.99% pure silver foil of thickness $H = 25$ μm or 50 μm mounted on an x–y translation stage in a vacuum chamber. Achromatic lenses coated for 800 nm and with focal lengths 100 mm, 150 mm, 200 mm, 250 mm, 300 mm, 400 mm and 500 mm were used. The pulse energy was changed with a neutral density filter set. The ablation depth per pulse, $d = H/N$, was estimated from the number of pulses, N, to just penetrate the foil, as seen from the transmitted intensity on a photodiode. The lens axial position was adjusted to minimize N to find the focus position.

The beam spatial profile was measured by the aperture method as well as with a Spiricon camera and found to be a good approximation to a Gaussian profile with a waist radius $\omega = 3.6$ mm at the focussing lens. The beam quality factor was measured to be $M^2 = 1.2 \pm 0.15$, which enabled the beam profile and hence the peak axial fluence, F, to be calculated at the focus. The peak fluence at the focus was also found from the measured radii, r_0, of holes drilled in the foil with different pulse energies [6,35]. These were found to be a good fit to the relation:

$$r_0^2 = \frac{\omega^2}{2} \ln\left(\frac{E}{E_{th}}\right) \quad (7)$$

so that the waist ω at the focus and hence the peak $F = 2E/\pi\omega^2$ could be found from the slope of r_0^2 versus $\ln(E)$. Absolute values of F were estimated to have an uncertainty of ±15%.

A Michelson interferometer, with one mirror that could be moved up to 800 mm, was used to generate double pulses with separations up to 3.4 ns. Co-linearity of the two Michelson beams was ensured by transmitting them over 10 m and checking the coincidence of the profiles to <0.2 mm on a Spiricon camera. The Michelson translation stage was not suitable for small separations so pulse separations from 0.2 ps to 6 ps were generated with an acousto-optic programmable dispersive filter (Fastlite, model Dazzler) inserted between the oscillator and the amplifier. A second harmonic generation intensity autocorrelator was used to check the pulse separation for the Dazzler and the zero crossing of the pulse separation from the Michelson interferometer.

4. Results and discussion

The *average* ablation depth per pulse to penetrate a 50 μm thick Ag foil as a function of peak *incident* fluence for a 200 mm focal length lens is shown in Fig. 5. The peak fluence was calculated from the waist diameter at the foil surface. This was measured from hole sizes to be 31 μm, similar to the value of 30.4 μm calculated from Gaussian beam propagation through the lens system. The results cover a very wide range of peak pulse fluence from 0.3 J cm^{-2} to 230 J cm^{-2} and a correspondingly wide range of ablation depths per pulse from 0.5 nm to 3500 nm. We consider four fluence regimes denoted A–D on Fig. 5.

Regimes A and B, corresponding to ablation depths per pulse up to a few 100 nm, have been widely studied experimentally and theoretically and are often referred to as the "low fluence" and "high fluence" regimes. More detailed measurements for these regimes are shown in Fig. 6. For regime B we find:

$$d = 85 \ln\left(\frac{F}{0.56}\right) \text{ nm} \quad \text{for } F \le 6.6 \text{ J cm}^{-2} \quad \text{or } d \le 239 \text{ nm}$$

This is in good agreement with previous measurements on Ag [3,7], as well as results for Cu [2] and Al. In contrast, we do not find

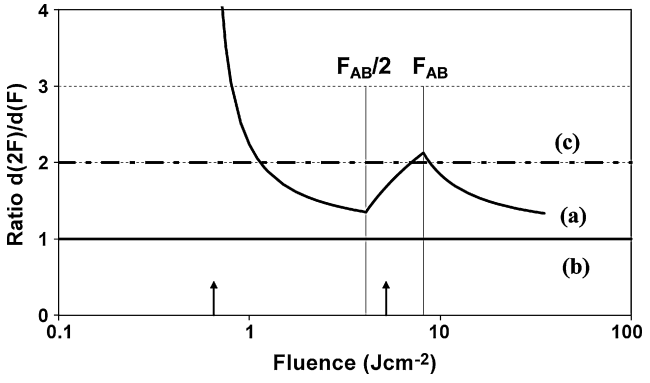

Fig. 4. Ratio of double to single pulse ablation depth as a function of pulse fluence F through a transition at fluence F_{AB} for (a) $\tau_S \to 0$, (b) complete absorption of the second pulse ($T_T = 0$) and (c) two independent pulses ($\tau_S \to \infty$). The arrows indicate the fluences corresponding to measurements in Fig. 8(a) and (d) and for the calculations in Fig. 11.

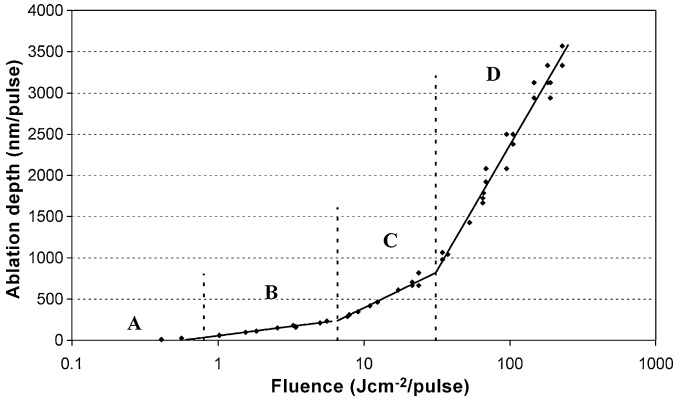

Fig. 5. Average ablation depth per pulse as a function of pulse fluence with different ablation regimes indicated.

Please cite this article in press as: D.E. Roberts, et al., Femtosecond laser ablation of silver foil with single and double pulses, Appl. Surf. Sci. (2009), doi:10.1016/j.apsusc.2009.10.004

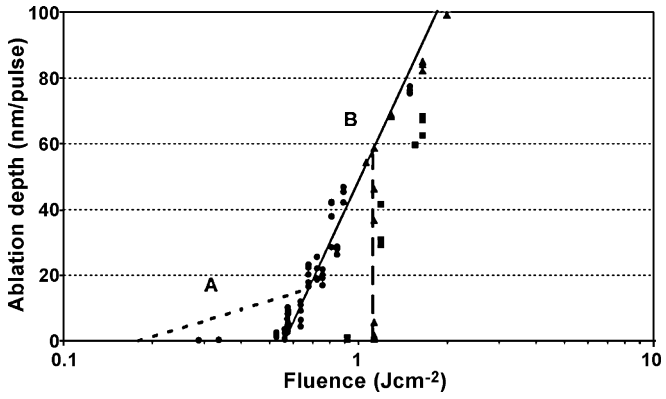

Fig. 6. Average ablation depth per pulse, d, as a function of pulse fluence for $d \leq 100$ nm. Circles, single pulse, other symbols for double pulses with the same total fluence, triangles with separation 4 ps, squares with separation 1.5 ps. Regime 'A' is not observed.

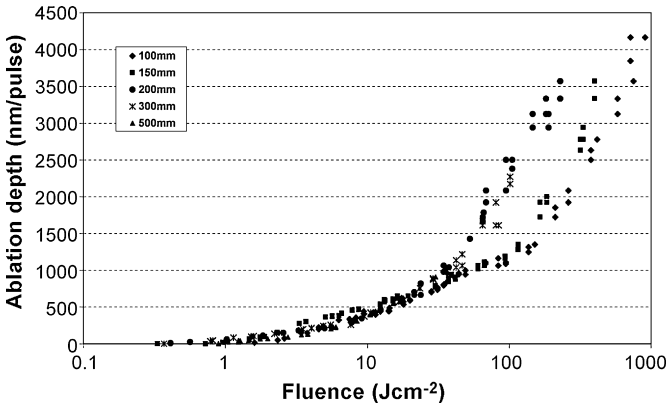

Fig. 7. Average ablation depth per pulse as a function of pulse fluence for different focussing lenses.

good agreement with earlier measurements in the low fluence regime, A, where the relation [2]:

$$d = 12 \ln\left(\frac{F}{0.18}\right) \text{nm}$$

is shown on Fig. 6 for comparison (here $\alpha^{-1} = 12$ nm for silver). In fact, we find our measurements continue to fit well to the regime B relation above, down to threshold at $F = 0.56$ J cm^{-2} (Fig. 6). We are unable to get penetration of the foil below this fluence. Actually, we are never able to achieve average ablation depths of <0.2 nm/pulse for this foil however long the foil is exposed to pulses with $F < 0.56$ J cm^{-2}.

A reason for this could be the difficulty of comparing *average* ablation depths from penetration of a relatively thick foil with depth measurements made from relatively shallow craters on a metal surface. Particularly near threshold, deep ablation with a Gaussian beam profile can lead to a high aspect ratio hole. This can pose problems limiting the ultimate depth achievable. These include differences in reflection coefficients, due to large angles of incidence at the sides of the hole, as well as re-entry of ejecta.

For a fluence profile $F(r) = F(0)\exp(-2r^2/\omega^2)$ and an ablation rate given by Eq. (1), the aspect ratio of the hole, A, can be estimated from $A = H/D$, where D is the diameter of the hole at half foil thickness, $H/2$. This gives $A = H/\omega/\sqrt{\ln(F(0)/F_{th}}$ or $A = H/\omega\sqrt{F_{th}/\delta F}$ where $F = F_{th} + \delta F$ and $\delta F \to 0$. Thus for $\omega = H = 25$ μm, $A > 5$ for $\delta F/F < 0.04$. This implies we ought to be able to see regime 'A' well above its threshold (see Fig. 6). However, the above estimate did assume a constant absorption of radiation across the hole radius. Other possible reasons for the absence of regime 'A' are that the absorptivity is nearer the very low classical value at low fluences or that, as indicated previously, electron diffusion is always dominant so $K = \alpha^{-1}$ in relation (1) is not appropriate.

Further measurements on the A and B regimes were done with the Dazzler to split each pulse into two equal intensity pulses each of half the single pulse fluence. With small pulse separations ≤4 ps, we find the dual pulse results in good agreement with the single pulse results for fluences down to ≈1.12 J cm^{-2}, i.e. twice the single pulse threshold. Below this it is impossible to get foil penetration so there is a large discontinuity in the d versus $\ln(F)$ characteristic at 1.12 J cm^{-2}. This is not consistent with the behaviour of two completely independent pulses, which would indeed have double the threshold fluence of the single pulse, i.e. $d = 2K\ln(F/2/F_{th})$ but then d would increase linearly with $\ln(F)$ with slope $2K$. Besides, 4 ps is much less than the electron phonon collision time, ≈10 ps for silver, so we should expect the same result as for the single pulse, i.e. $d = K\ln((F/2 + F/2)/F_{th})$. These results imply a strong incubation effect of the first pulse though not of the form normally assumed in damage studies [35].

Like regime B, the results in regimes C and D fit well to logarithmic dependencies (1) (Fig. 5):

Regime C:	$d = 376\ln(F/3.5)$ nm for 6.6 J cm$^{-2} \leq F \leq$ 31.1 J cm^{-2}	(or 239 nm ≤ d ≤ 822 nm)
Regime D:	$d = 1323\ln(F/16.7)$ nm for 31.1 J cm$^{-2} \leq F$	(or 822 nm ≤ d)

These very high fluence regimes for $d >$ a few 100 nm have been much less widely studied. What is striking for all our measurements is that the transition between the regimes shows, within experimental errors, quite a distinctive change of slope over a very narrow fluence range, though no evidence of a discontinuous jump in the ablation depth.

Results with different focal length lenses, but still as a function of peak fluence on the beam axis, are shown in Fig. 7. In all cases, good fits to a logarithmic fluence dependence are found together with sharp changes in slope at well defined fluences, F_T. The best fit K and F_{th} to the measurements are summarized in Table 1, together with the transition fluences, F_T, for crossover between two regimes. These show that the approximately 30–200 nm ablation range seems to be largely independent of the beam spot size while the high fluence regime as well as the cut-off fluence in the regime of $d < 20$ nm depends on the beam spot size.

In order to study one of the transition regimes, double pulse ablation measurements were made as a function of pulse separation and pulse fluence spanning the transition regime at the lowest fluence. All measurements were made with both pulses having the same energy and quoted fluences are for each *single* pulse. Results are shown in Fig. 8 together with the single pulse ablation results for comparison.

At the lowest fluence and for pulse separation $\tau_s \to 0$, $d(2F) \approx 85$ nm, much larger than the single pulse ablation depth $d(F) \approx 12$ nm (Fig. 5(a)). This large ratio of $d(2F)/d(F) \approx 7$ is consistent with the near threshold estimate shown arrowed in Fig. 4 and is completely different from the result (= 2) for two independent pulses. As τ_S is increased, $d(2F)$ decreases only slowly up to $\tau_S \approx 8$ ps before decreasing approximately exponentially to the single pulse value with a decay time, τ_{de}, of about 130 ps. For $\tau_S > 700$ ps, $d(2F) \approx d(F)$. In this case, *and in all subsequent measurements*, the maximum τ_S used (3.4 ns) was not sufficient to reach the regime of two independent pulses (i.e. $d(2F) = 2d(F)$).

As the fluence is increased (Fig. 8(b)–(g)), the ratio $d(2F)/d(F)$ decreases for $\tau_S \to 0$, in accordance with the estimates in Fig. 4(a). For example, for $F = 5.9$ J cm^{-2}, the measured ratio $d(2F)/$

Please cite this article in press as: D.E. Roberts, et al., Femtosecond laser ablation of silver foil with single and double pulses, Appl. Surf. Sci. (2009), doi:10.1016/j.apsusc.2009.10.004

Table 1
Best fit parameters, K and F_{th}, in Eq. (1) for different logarithmic fluence regimes and transition fluences, F_T, for different spot sizes on the sample (*f.l.* = focal length of lens, omega = beam waist radius on sample).

f.l. (mm)	Omega (μm)	Regime B		Regime C		Regime D
		K/F_{th} (nm/J cm^{-2})	F_T (J cm^{-2})	K/F_{th} (nm/J cm^{-2})	F_T (J cm^{-2})	K/F_{th} (nm/J cm^{-2})
100	7.6			336/2.8	165.8	1583/69.7
150	11.4	147/0.89	2.9	277/1.6	110.4	1591/52.3
200	15.2	85/0.56	6.0	376/3.5	31.1	1323/16.7
250	19.0	137/0.70	9.1	398/3.7	[a]	[a]
300	22.8	109/0.57	8.0	471/4.4	[a]	[a]
400	30.4	81/0.56	3.4	275/2.0	[a]	[a]
500	38.0	84/0.81	6.7	474/4.6	[a]	[a]

[a] Not accessible due to insufficient laser power.

$d(F) = 1.45$ for $\tau_S \to 0$ which is consistent with the (second) arrowed value in Fig. 4(a). Another feature of increasing fluence is that both the time for which $d(2F)$ stays approximately constant with τ_s, as well as the decay time to $d(F)$, decrease substantially. Near the transition fluence, 9 J cm^{-2}, the total time for $d(2F)$ to reach $d(F)$ is only ≈3.2 ps, a decrease of a factor of 200 from the low fluence case. The rapid decrease with fluence of both the time, τ_C, for which $d(2F) \approx d(F)$ and the decay time, τ_{de}, are shown in Fig. 9.

We now consider the results above the transition fluence. A significant change is that the time for which $d(2F) \to d(F)$ is now very large so there is a discontinuity in this time across the transition fluence (Fig. 8(e)–(g)). This appears to be the first evidence of a discontinuity through an ablation transition regime. A distinctive feature above the transition fluence is that for small τ_S, $d(2F)$ increases with τ_S. This is particularly noticeable at the highest fluence studied (Fig. 8(g)). Use of the Michelson led to half the transmitted energy compared with when it was bypassed for single pulse measurements and for Dazzler double pulse measurements, so higher fluences were not accessible for $\tau_s > 6$ ps.

Another distinctive feature of the double pulse results is that the ablation depth does not always simply fall to the single pulse depth with increasing τ_S but can fall significantly *below* this depth before rising again to near the single pulse depth as τ_s is further increased. This is particularly striking at a (single pulse) fluence of 1.3 J cm^{-2} where, for a pulse separation of 1000 ps, the minimum *double* pulse ablation depth is only 40% of the *single* pulse depth (Fig. 8(b)). This effect seems to have been observed before (Fig. 2 of Ref. [27]) as well as in the lowering of a nanoparticle intensity signal caused by a second pulse [29]. A plot of the ratio $d(2F)/d(F)$ versus fluence for two different τ_S (Fig. 10) shows a gradual increase in the ratio for increasing fluence above 1.3 J cm^{-2}.

To understand these results, we first consider the calculations with the two temperature model at the lowest measured fluence. A simple interpretation of the logarithmic fluence dependence (1), consistent with the *basic* two temperature model with a *critical temperature* for ablation, is that the maximum lattice surface temperature varies with depth as $T_{imax}(z) = T_{imax}(0)\exp(-z/L)$. Here L is an effective diffusion length. If the ablation depth per pulse, d, is then equated to the depth at which $T_{imax} = T_{ab}$, we have $d = L\ln(T_{imax}(z=0)/T_{ab})$.

We can thus estimate d as a function of τ_S using the calculated maximum temperatures, as shown for one specific fluence in Fig. 3, and L = 145 nm (i.e. similar to the experimentally measured values of K in Table 1 and typical diffusion lengths given in Ref. [3]). Calculated results for low fluence, shown in Fig. 11(a), are in remarkably good agreement with the measured values shown in Fig. 8(a). Specifically, $d(2F) = 85$ nm, as observed though $d(F) = 22$ nm is higher. Therefore the ratio of $d(2F)/d(F)$ for $\tau_S \to 0$ is not as large as observed, though still much higher than the ratio (= 2) for independent pulses. The calculated time for which d remains approximately constant is about 10 ps (i.e. $\approx\tau_{ei}$), after which the electron and lattice temperatures are approximately equal (Fig. 1). The calculated d then decays over a longer time scale of ≈100 ps following the diffusion rate used in the present calculation. By this time the heat pulses are well separated (Fig. 1(d)). It therefore appears that the ablation of material from the first pulse is too small and occurs on too slow a time scale to affect the absorption of laser energy by the second pulse. The calculated time scales for d versus τ_S are in very good agreement with the experimental results.

Estimates of d from the above relation for a larger fluence, F = 5.9 J cm^{-2}, with the same L = 145 nm are shown in Fig. 11(b). The agreement is now much poorer though the basic observations of a considerably larger d than at low fluence and a much smaller ratio of $d(2F)/d(F)$ for $\tau_s \to 0$ are still preserved. However, the calculated timescale of the decay from $d(2F)$ to $d(F)$ is almost the same as in the low fluence case and completely different from the measured decay time of a few ps only (Fig. 8(d)). It therefore appears possible that double (equal) pulse ablation measurements can only give clear information about electron–phonon coupling times and diffusion times at rather low fluences and that at high fluences the observed decay time is a convolution of different time constants in the ablation process. Of particular interest for further study would be the case where the first pulse is below threshold for ablation but the second pulse raises the substrate temperature to above threshold for ablation. Then there would not be complications due to the second pulse penetrating ejecta from the first pulse.

In general, the trend of the estimated τ_{ei} with fluence is not in agreement with experiment (Fig. 9). A possible reason for the shorter constant d versus τ_S region would be a stronger temperature dependence for the electron–phonon coupling parameter, g, than used here. For example, the model used in Ref. [13] has $g = g_0(A/B(T_e + T_i) + 1)$ which would give a much larger g at high temperatures and a correspondingly shorter τ_{ei} at higher fluences. Nevertheless, this would not explain the fast decay time from $d(2F)$ to $d(F)$. An indication of why this happens is given by the reduction of the double pulse ablation depth to significantly *below* the single pulse depth for a pulse separation of about 1000 ps with F = 1.3 J cm^{-2} (Fig. 10). This could be due to ejected particles from the first pulse being driven back to the substrate by the second pulse.

We note that femtosecond laser ablated material has been shown to comprise three distinct groups of species: ions with typical velocities from the surface of about 4×10^4 m/s, neutrals with velocities of about 10^4 m/s, and nano and mesoparticles with velocities of less than about 300 m/s [33–38]. Therefore, in the above case, the heavier particles ablated by the first pulse will have moved only ≈300 nm from the substrate surface by the time the second pulse arrives.

Since most of the ablated mass is in the form of nano and mesoparticles, absorption of radiation from the second pulse, on the surface of nano and mesoparticles ejected by the first pulse, might cause sufficient ablation to generate enough momentum to

Please cite this article in press as: D.E. Roberts, et al., Femtosecond laser ablation of silver foil with single and double pulses, Appl. Surf. Sci. (2009), doi:10.1016/j.apsusc.2009.10.004

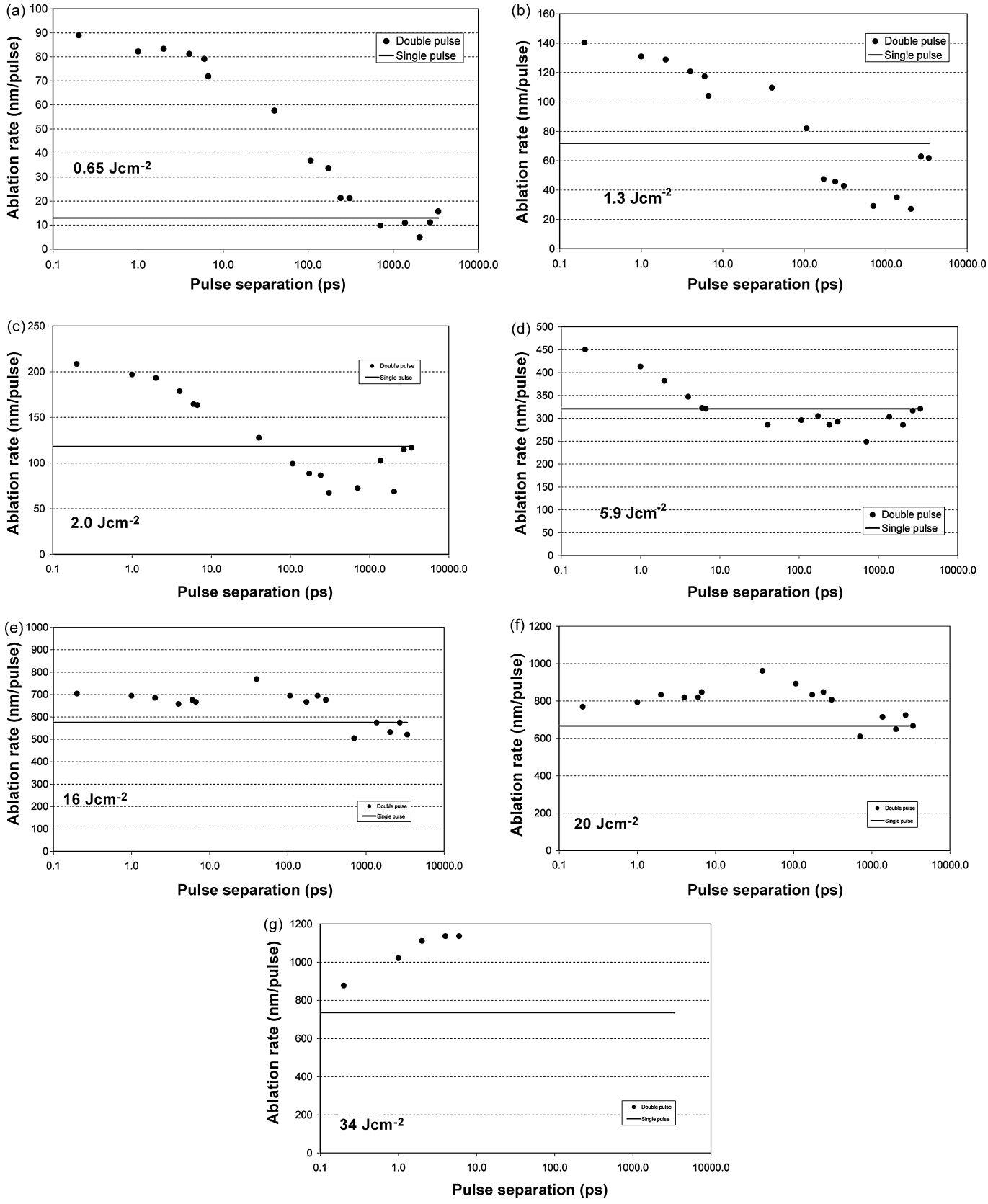

Fig. 8. Average ablation depth per pulse as a function of pulse separation for different single pulse fluences.

Please cite this article in press as: D.E. Roberts, et al., Femtosecond laser ablation of silver foil with single and double pulses, Appl. Surf. Sci. (2009), doi:10.1016/j.apsusc.2009.10.004

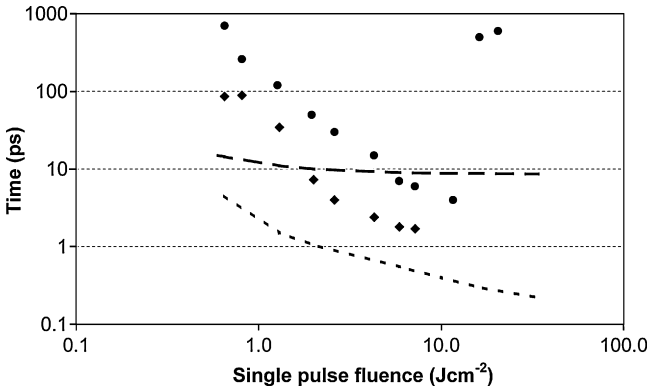

Fig. 9. Circles: measured time, τ_C, for which double pulse ablation depth approximately equals the single pulse depth. Diamonds: measured decay time, τ_{de}, from double to single pulse ablation depth. Dashed line: calculated time, τ_{ei}, for lattice temperature to reach 99% of electron temperature. Dotted line: calculated time for lattice temperature to reach ablation temperature, T_{ab}.

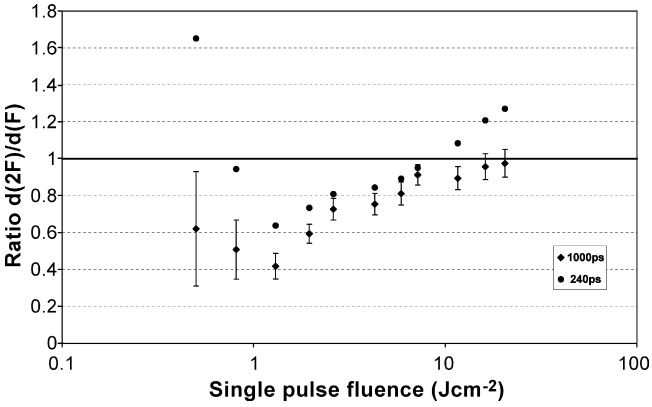

Fig. 10. Ratio of double to single pulse ablation, for pulse separations of 240 ps and 1000 ps, showing the double pulse depth falling below the single pulse depth.

drive the particle back to the surface. We can make a simple estimate of the magnitude of this repulsion by assuming the reverse momentum of the particle is proportional to the energy it absorbs from the second pulse. This can then be related to the momentum of the plume generated by the first pulse if we assume the angular spread of the plume is small, as observed [37]. For a single pulse with ablation depth d, the total ablated mass is $Ad\rho$ and the plume momentum $Ad\rho v_{out}$. This assumes an ablated area A and that most of the mass in the plume is in nanoparticles of mean speed $\boldsymbol{v}_{out}$. The momentum has been generated by an absorbed energy $(1-R)AF$.

A nanoparticle of radius r exposed to the second pulse will absorb an energy $Q_{abs}\pi r^2 F$, where Q_{abs} is the absolute absorption crosssection of the particle divided by its projected area, πr^2. The absorption would be on the particle surface facing the second pulse. The particle momentum is then

$$\frac{4}{3}\pi r^3 \rho v_{in} \approx \frac{Q_{abs}\pi r^2 F}{(1-R)AF} \times Ad\rho v_{out} \tag{8}$$

where $\boldsymbol{v}_{in}$ is the speed of the particle towards the substrate. Thus:

$$\frac{v_{in}}{v_{out}} = \frac{3}{4}\left(\frac{Q_{abs}}{1-R}\right)\frac{d}{r} \tag{9}$$

The ratio $Q_{abs}/(1-R)$ can be estimated from a Mie scattering calculation for Q_{abs} [42] with the same complex refactive index of silver, $\mu = 0.0312 + 5.194i$ at 795 nm, for Q_{abs} and $(1-R)$.

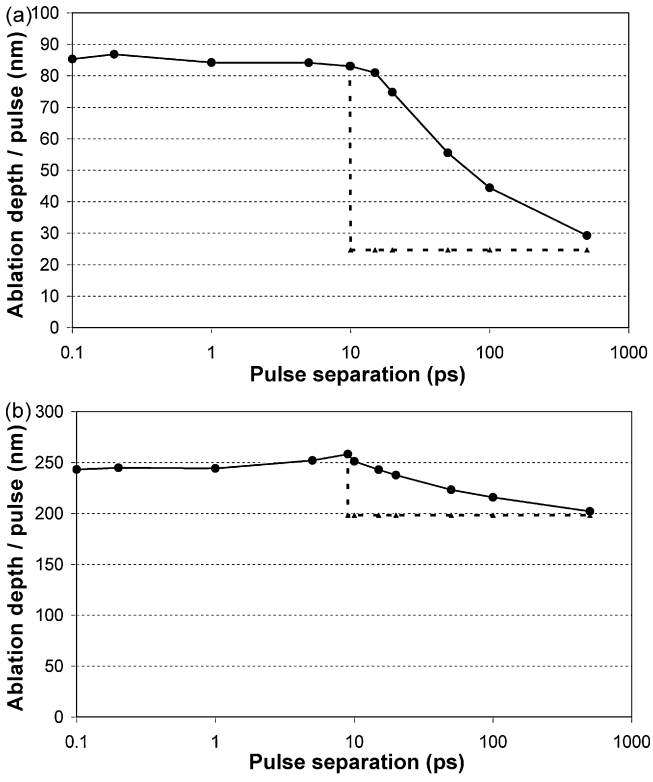

Fig. 11. Ablation depth per pulse estimated from peak surface temperature versus pulse separation. Solid line: from double pulse. Dashed line: from first pulse. (a) $F = 0.65$ J cm^{-2} (compared with Fig. 8(a)) and (b) $F = 5.9$ J cm^{-2} (compared with Fig, 8(d)).

For nanoparticles with $r < 20$ nm, $Q_{abs} \approx Cr$, where C is a constant ($= 5 \times 10^{-5}$, see Fig. 12) since then, approximately, $r < \Lambda$ ($= \lambda/4\pi k$) the characteristic absorption length in the material. This yields $\boldsymbol{v}_{in}/\boldsymbol{v}_{out} = 0.011d$, essentially independent of the size of the nanoparticle. Thus $\boldsymbol{v}_{in} > \boldsymbol{v}_{out}$ for $d > 90$ nm, similar to the single pulse $d = 72$ nm in Fig. 8(b). A problem with considering smaller particles, however, is that most of the ablation should occur over a depth Λ so that complete ablation of the particle may occur before it strikes the surface. This suggests larger particles may play a role in the re-deposition.

Measurements of nanoparticle size distributions vary over quite a large range with peaks of the distributions typically at radii of 5–20 nm [37,39–41]. However, nickel mesoparticles as large as ~100 nm radius have been observed in femtosecond ablation at

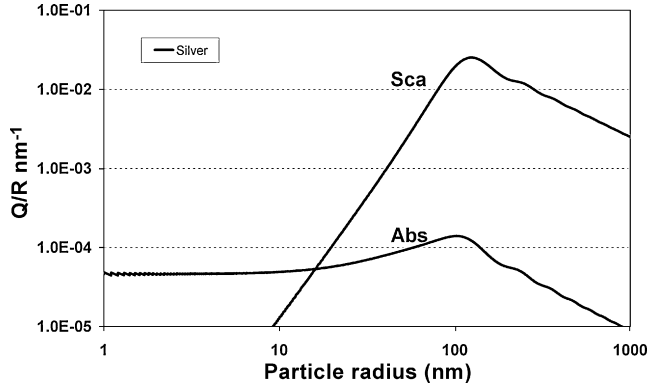

Fig. 12. Spherical particle absorption efficiency, Q_{abs}, and scattering efficiency, Q_{sca}, divided by radius as a function of radius for silver.

Please cite this article in press as: D.E. Roberts, et al., Femtosecond laser ablation of silver foil with single and double pulses, Appl. Surf. Sci. (2009), doi:10.1016/j.apsusc.2009.10.004

8 J cm^{-2} [41] while in Ref. [29] a very broad distribution of Ti nanoparticles was found with a median radius of 25 nm but particles with radii up to 250 nm being detected. Metal blobs on the micron scale are also ejected at high fluences [36]. The peak particle absorption efficiency for Mie scattering of silver occurs for a radius of about 118 nm (Fig. 12).

Thus it seems likely that a large fraction of the 60% of ejecta repelled back to the substrate seen in the present work is in the form of much larger particles, i.e. with radii near 100 nm, than the dominant sizes typically measured for nanoparticles. Since the scattering crosssection of large particles is also very large (Fig. 12), incident light scattering as well as absorption would cause considerable interference with the propogation of the second pulse. We note that the reduction of the net ablation depth by a second pulse interacting with nanoparticles may not be a desirable scenario for double pulse LIBS interpretation. Different species could have different percentages of nanoparticle formation and different size distributions so the direct relation of atomic line intensities to species concentration may not be valid.

The present measurements are insufficient to do more than speculate about what happens at high fluences. The reduction in measured times with fluence seen in Fig. 9 correlate with a reduction of the time for the surface of the substrate to reach critical temperature. Therefore, while the second pulse sees a strongly heated but relatively unperturbed lattice at low fluence this is not likely to be the case at higher fluences. The percentage of ablated mass that is repelled back to the substrate decreases with increasing fluence (Fig. 8). This could be due to a combination of factors: increasing momentum in the ablation plume, increasing breakup of nanoparticles etc.

It seems likely that the large jump in times in Fig. 9 is due to a marked phase change in the ablation products, i.e. the ablated mass varies continuously across the transition but the composition changes from a predominantly particle to a predominantly atomic component. The absorption of the second pulse would then be by ionisation and inverse Bremsstrahlung, etc., rather than by Mie scattering.

5. Conclusion

We have found several marked changes of slope of the femtosecond laser ablation depth versus logarithmic fluence dependence of silver foil. One of these transition regimes has been probed using a second collinear, delayed pulse. At low fluence, the double pulse ablation depth is independent of pulse separation up to about the electron lattice relaxation time. With increasing pulse separation, the ablation depth falls to the single pulse value on an electron diffusion timescale. At higher fluences ejecta from the first pulse interfere with the second pulse and timescales are affected by absorption and scattering of radiation by emitted nano and mesoparticles.

References

[1] B.N. Chichkov, C. Momma, S. Nolte, F. von Alvensleben, A. Tünnermann, Appl. Phys. A 63 (1996) 109–115.
[2] S. Nolte, C. Momma, H. Jacobs, A. Tünnermann, B.N. Chichkov, B. Wellegehausen, H. Welling, J. Opt. Soc. Am. B 14 10 (1997) 2716–2722.
[3] K. Furusawa, K. Takahashi, H. Kumagai, K. Midorikawa, M. Obara, Appl. Phys. A 69 (Suppl.) (1999) S359–S366.
[4] K. Venkatakrishnan, B. Tan, B.K.A. Ngoi, Opt. Laser Technol. 34 (2002) 199–202.
[5] M. Hashida, A.F. Semerok, O. Gobert, G. Petite, Y. Izawa, J.F. Wagner, Appl. Surf. Sci. 197–198 (2002) 862–867.
[6] P.T. Mannion, J. Magee, E. Coyne, G.M. O'Connor, Proc. SPIE 4876 (2003) 470–478.
[7] P.T. Mannion, S. Favre, C. Mullan, D.S. Ivanov, G.M. O'Connor, T.J. Glynn, B. Doggett, J.G. Lunney, J. Phys.: Conf. Ser. 59 (2007) 753–759.
[8] B. Hüttner, J. Phys.: Condens. Matter 10 (1998) 6121–6126.
[9] Z. Lin, L.V. Zhigilei, Appl. Surf. Sci. 253 (2007) 6295–6300.
[10] A. Miotello, R. Kelly, Appl. Phys. A 69 (Suppl.) (1999) S67–S73.
[11] L.V. Zhigilei, Appl. Phys. A 76 (2003) 339–350.
[12] C. Cheng, X. Xu, Phys. Rev. B 72 (2005) 165415.
[13] J. Yang, Y. Zhao, X. Zhu, Appl. Phys. A 89 (2007) 571–578.
[14] L.V. Zhigilei, Z. Lin, D.S. Ivanov, J. Phys. Chem. C 113 (2009) 11892–11906.
[15] K. Sokolowski-Tinten, J. Bialkowski, A. Cavalleri, D. von der Linde, Phys. Rev. Lett. 81 (1) (1998) 224–227.
[16] J. Hohlfeld, S.-S. Wellershoff, J. Güdde, U. Conrad, V. Jähnke, E. Matthias, Chem. Phys. 251 (2000) 237–258.
[17] O. Andrusyak, M. Bubelnik, J. Mares, T. McGovern, C.W. Siders, Proc. SPIE 5647 (2005) 61–67.
[18] K. Kawahara, Y. Kurogi, N. Matsuo, T. Ninomiya, H. Sawada, A. Yokotani, K. Kurosawa, Proc. SPIE 4830 (2003) 526–530.
[19] R. Le Harzic, D. Breitling, S. Sommer, C. Föhl, K. König, F. Dausinger, E. Audouard, Appl. Phys. A 81 (2005) 1121–1125.
[20] V. Hommes, M. Miclea, R. Hergenröder, Appl. Surf. Sci. 252 (2006) 7449–7460.
[21] S.M. Angel, D.N. Stratis, K.L. Eland, T. Lai, M.A. Berg, D.M. Gold, Fresenius J. Anal. Chem. 369 (2001) 320–327.
[22] V.I. Babushok, F.C. DeLucia Jr., J.L. Gottfried, C.A. Munson, A.W. Miziolek, Spectrochim. Acta B 61 (2006) 999–1014.
[23] J.T. Schiffern, D.W. Doerr, D.R. Alexander, Spectrochim. Acta B 62 (2007) 1412–1418.
[24] V. Piñon, C. Fotakis, G. Nicolas, D. Anglos, Spectrochim. Acta B 63 (2008) 1006–1010.
[25] S. Singha, Z. Hu, R.J. Gordon, J. Appl. Phys. 104 (2008) 113520.
[26] T.Y. Choi, D.J. Hwang, C.P. Girgoropoulos, Appl. Surf. Sci. (2002) 720–725.
[27] A. Semerok, C. Dutouquet, Thin Solid Films 453–454 (2004) 501–505.
[28] I.H. Chowdhury, X. Xu, A.M. Wiener, Appl. Phys. Lett. 86 (2005) 151110.
[29] D. Scuderi, D. Moreau, O. Albert, P.P. Pronko, J. Etchepare, Appl. Surf. Sci. 248 (2005) 309–312.
[30] Z. Han, C. Zhou, E. Dai, J. Xie, Opt. Commun. 281 (18) (2008) 4723–4726.
[31] S. Noël, E. Axente, J. Hermann, Appl. Surf. Sci. 255 (2009) 9738–9741.
[32] Z. Lin, L.V. Zhigilei, V. Celli, Phys. Rev. B 77 (2008) 075133–75217.
[33] B.H. Christensen, K. Vestentoft, P. Balling, Appl. Surf. Sci. 253 (2007) 6347–6352.
[34] N.M. Bulgakova, I.M. Burakov, Y.P. Meshcheryakov, R. Stoian, A. Rosenfeld, I.V. Hertel, J. Las. Micro/Nano Eng. 2 (2007) 76–86.
[35] S.E. Kirkwood, A.C. van Popta, Y.Y. Tsui, R. Fedosejevs, Appl. Phys. A 81 (2005) 729–735.
[36] S. Bruneau, J. Hermann, G. Dumitru, M. Sentis, E. Axente, Appl. Surf. Sci. 248 (2005) 299–303.
[37] S. Amoruso, G. Ausanio, R. Bruzzese, L. Gragnaniello, L. Lanotte, M. Vitiello, X. Wang, Appl. Surf. Sci. 252 (2006) 4863–4870.
[38] D. Scuderi, R. Benzerga, O. Albert, B. Reynier, J. Etchepare, Appl. Surf. Sci. 252 (2006) 4360–4363.
[39] S. Amoruso, G. Ausanio, A.C. Barone, R. Bruzzese, C. Campana, X. Wang, Appl. Surf. Sci. 254 (2007) 1012–1016.
[40] S. Noël, J. Hermann, T. Itina, Appl. Surf. Sci. 253 (2007) 6310–6315.
[41] B. Liu, Z. Hu, Y. Che, Y. Chen, X. Pan, Appl. Phys. Lett. 90 (2007) 044103.
[42] C.F. Bohren, D.R. Huffman, Absorption and Scattering of Light by Small Particles, Wiley–VCH, Berlin, 1998.

Please cite this article in press as: D.E. Roberts, et al., Femtosecond laser ablation of silver foil with single and double pulses, Appl. Surf. Sci. (2009), doi:10.1016/j.apsusc.2009.10.004